00

Modeling radiation of transfer in multilayered tissue taking into account surface curvature

© Yu.A. Zhavoronkov, S.V. Ul'yanov ¶, R.R. Chegadaev

St. Petersburg State University,
St. Petersburg, Russia

¶ e-mail: ulyanov_sv@mail.ru

Received June 11, 2025
Revised July 28, 2025
Accepted November 25, 2025

Modeling of the backscatter intensity of infrared laser radiation on two-layer and four-layer randomly inhomogeneous tissue was performed. A human head model was used as the primary object of study. The results of a comparison of simulations performed for two limiting cases are presented: flat infinite layers of finite thickness and a layered structure with hemispherical boundaries. Radiation transfer in biological tissue was modeled using the Bethe–Salpeter equation in the ladder approximation. The dependences of the backscatter intensity on the distance between the radiation entry point and the photon exit point were obtained. The influence of skull curvature and thickness on the scattering intensity was studied. It was shown that backscatter data can be used in the diagnosis of intracranial injuries.

Keywords: backscattering, Monte Carlo simulation, Bethe–Salpeter equation, multilayer tissue.

DOI: 10.61011/EOS.2025.12.63175.38-25

1. Introduction

The transfer of the near-infrared laser radiation in biological media has been the focus of researcher's interest for a long time [1,2]. This is primarily due to the possibility of using tissue-scattered radiation in medical applications. This kind of radiation, which is safe for the human body, is characterized by a low absorption coefficient, and the equipment used is relatively simple and inexpensive.

As a rule, three main types of incident radiation are used in research: continuous [3–7], short-pulse [8–13], as well as waves with various radiation modulation options [13–16].

In this paper, we consider the case when the studied object — a human head model, is irradiated with a continuous infrared laser beam. For a correct description of radiation scattering in this model, it is necessary to allow for the change in optical parameters across the tissue depth, i.e. use a multilayer structure of the skull and underlying tissues. In studies [6,17,18] the calculations were made for a 2-layer model of „skull–brain", and in [19] — for a 4-layer model of „skin–skull–cerebrospinal fluid (CSF)–brain".

The intensity of the backscattered laser radiation was determined by iteratively solving the Bethe–Salpeter equation [20,21], and the terms of the iterative series correspond to different multiplicities of scattering. Each of them was modeled using Monte Carlo method based on the widely used MCML [22] technique, while the layers were assumed to be planar. Choosing the Bethe–Salpeter equation method to describe the radiation transfer in a randomly inhomogeneous medium is explained by its general applicability, including for accounting for interference effects in the scattering processes. In contrast to the computationally simpler diffusion approximation, the Bethe– Salpeter equation allows us to correctly describe the scattering of small orders in which the transport length has not yet been formed. The first successful implementations of Monte Carlo method based on the iterative solution of Bethe–Salpeter equation were given in papers [23–26].

The strictly backscattered intensity dependence on the distance between the source and receiver located on the head surface was studied in [6, 19]. The modified MCML algorithm allowed to take into account the contribution of each aspect of the scattering process into the total intensity which significantly diminished the calculations time [27,28].

In the present study, this technique was extended to the case of models taking into account the actual curvature of the layers. The upper part of the head was modeled as a hemisphere, and the boundaries between the tissue layers were taken as spherical. The dependences of the backscattering intensity on the distance between the source and receiver are compared for models with plane and spherical boundaries. To account for the scattering anisotropy, the Henyey–Greenstein phase function was used.

2. Radiation transfer

The transfer of steady-state radiation in an infinite randomly inhomogeneous medium may be characterized by

the Bethe–Salpeter equation in the „ladder" approximation:

$$\Gamma(\mathrm{r}_2, \mathrm{r}_1|\mathrm{k}_s, \mathrm{k}_i) = \frac{k_0^4}{4\pi^2} G(\mathrm{k}_s - \mathrm{k}_i)\delta(\mathrm{r}_2 - \mathrm{r}_1)$$

$$+ \frac{k_0^4}{4\pi^2} \int d\mathrm{r}_3\, G(\mathrm{k}_s - \mathrm{k}_{23})\Lambda(\mathrm{r}_2 - \mathrm{r}_3)\Gamma(\mathrm{r}_3, \mathrm{r}_1|\mathrm{k}_{23}, \mathrm{k}_i), \quad (1)$$

where coherence function $\Gamma(\mathbf{r}_2, \mathbf{r}_1|\mathbf{k}_s, \mathbf{k}_i)$ describes propagation of radiation incident at point $\mathbf{r}_1$ and emerging at point $\mathbf{r}_2$ with the initial wave vector $\mathbf{k}_i$ and final wave vector $\mathbf{k}_s$; $\mathbf{k}_{ij} = k_0\mathbf{r}_{ij}/r_{ij}$, $\mathbf{r}_{ij} = \mathbf{r}_i - \mathbf{r}_j$, $k_0 = 2\pi/\lambda$ — wave number, λ — wavelength in vacuum. The product of two complex-conjugate average Green's functions of a scalar field yields single scattering propagator: $\Lambda(r) = r^{-2}\exp(-\mu r)$, where $\mu = \mu_s + \mu_a$ — extinction coefficient. $G(\mathbf{k})$ is the Fourier transform of the correlation function of permittivity fluctuations:

$$G(\mathbf{k}) = \int d(\mathbf{r} - \mathbf{r}_0)\, e^{-i\mathbf{k}\cdot(\mathbf{r}-\mathbf{r}_0)} \langle \delta\varepsilon(\mathbf{r})\, \delta\varepsilon^*(\mathbf{r}_0)\rangle.$$

The optical theorem relates the scattering coefficient μ_s to the integral intensity of a single scattering. Both values are expressed in terms of the correlation function $G(\mathbf{k})$; in particular, for a scalar field:

$$\mu_s = \frac{k_0^4}{(4\pi)^2} \int d\Omega_s\, G(\mathbf{k}_s - \mathbf{k}_i). \quad (2)$$

Having introduced the normalized phase function

$$p(\hat{\mathbf{k}}_s, \hat{\mathbf{k}}_i) = \frac{G(\mathbf{k}_s - \mathbf{k}_i)}{\int d\Omega_s\, G(\mathbf{k}_s - \mathbf{k}_i)},$$

where $\hat{\mathbf{k}}$ — unit vector along the wave vector $\mathbf{k}$, equation (1) may be rewritten as:

$$\Gamma(\mathbf{r}_2, \mathbf{r}_1\,|\,\mathbf{k}_s, \mathbf{k}_i) = \mu_s p(\hat{\mathbf{k}}_s, \hat{\mathbf{k}}_i)\delta(\mathbf{r}_2 - \mathbf{r}_1)$$

$$+ \mu_s \int d\mathbf{r}_3\, p(\hat{\mathbf{k}}_s, \hat{\mathbf{k}}_{23})\Lambda(\mathbf{r}_2 - \mathbf{r}_3)\Gamma(\mathbf{r}_3, \mathbf{r}_1\,|\,\mathbf{k}_{23}, \mathbf{k}_i). \quad (3)$$

Note that the phase function depends only on the cosine of angle θ between the corresponding vectors: $p(\hat{\mathbf{k}}_s, \hat{\mathbf{k}}_i) = p(\cos\theta)$.

Let z be the Cartesian coordinate of point $\mathbf{r} = (\mathbf{r}_\perp, z)$ perpendicular to the boundaries of a plane-parallel layer with thickness T, $0 \leqslant z \leqslant T$, including the case of a semi-infinite medium at $z \geqslant 0$. Within a constant dimensional factor, the main incoherent part of intensity of radiation scattered into the upper half-space (further in the text — „backscattered") radiation is [28–30]:

$$J(\mathbf{k}_i, \mathbf{k}_s) = 4\pi \int_0^\infty dz_1 \int_{z_2>0} d\mathbf{r}_2\, \Gamma(\mathbf{r}_2, \mathbf{r}_1\,|\,\mathbf{k}_s, \mathbf{k}_i)$$

$$\times \exp\left(-\mu\left(\frac{z_2}{\cos\theta_s} + \frac{z_1}{\cos\theta_i}\right)\right),$$

where θ_i is the incidence angle and θ_s is the backscattering angle measured from the direction opposite to axis z.

The iterative solution of Bethe–Salpeter equation (3) yields a representation of intensity in the form of a series in scattering multiplicities:

$$J(\mathbf{k}_i, \mathbf{k}_s) = \sum_{n=1}^{\infty} J^{(n)}(\mathbf{k}_i, \mathbf{k}_s), \quad (4)$$

where $J^{(n)}(\mathbf{k}_i, \mathbf{k}_s)$ — is the contribution of the nth scattering order.

Within the ladder approximation the term of n-th order $J^{(n)}(\mathbf{k}_i, \mathbf{k}_s)$ may be presented as an average over sample of N_{ph} incident photons:

$$J^{(n)}(\mathbf{k}_i, \mathbf{k}_s) = \frac{1}{N_{\mathrm{ph}}} \sum_{j=1}^{N_{\mathrm{ph}}} W_n^{(j)}(\mathbf{k}_i, \mathbf{k}_s)$$

$$\times\, p\left(\hat{\mathbf{k}}_{n\,n-1}^{(j)}, \hat{\mathbf{k}}_s\right) f_{\mathrm{BLB}}(\mathbf{k}_i, \mathbf{k}_s, z_1^{(j)}, z_n^{(j)}), \quad (5)$$

where $W_n^{(j)}(\mathbf{k}_i, \mathbf{k}_s)$ — weight of the appropriate trajectory, $z_n^{(j)}$ — coordinate of the point of n-th scattering $\mathbf{r}_n^{(j)}$.

Bouger–Lambert–Beer multiplier

$$f_{\mathrm{BLB}}(\mathbf{k}_i, \mathbf{k}_s, z_1^{(j)}, z_n^{(j)})$$

describes the exponential decay of radiation along the path from the entry point to the first scattering and from the nth scattering point to the exit from the medium. It depends on the optical properties of the medium in the path of the photons, as well as on the geometry of the trajectory.

The weight $W_n^{(j)}$ is a random realization of a multiple spatial integral that occurs during the iterative solution of the Bethe–Salpeter equation. To calculate it, a stochastic sequence (trajectory) of scattering points is modeled: $\mathbf{r}_1, \ldots, \mathbf{r}_n$.

3. Modeling of multiple light scattering in biological tissue for plane-parallel layers

An alternative to the analytical solution of the Bethe–Salpeter is a Monte Carlo simulation of multiple scattering. This method is based on using the inverse transform procedure. Integrals over a semi-infinite interval are reduced to integrals over a unit interval. The single scattering propagator shows that the photon's mean free path obeys an exponential distribution law with a probability density $f(r) = \mu\exp(-\mu r)$ over the interval $r \in [0, +\infty)$, where r is the distance between neighboring scattering points. For such a density, the cumulative distribution function $\xi = F(r)$ is calculated as follows:

$$\xi = \int_0^r f(r')dr' = 1 - \exp(-\mu r). \quad (6)$$

Inverse transform $r = F^{-1}(\xi)$ gives:

$$r = -\mu^{-1}\ln(1-\xi) = -\mu^{-1}\ln\xi', \tag{7}$$

where ξ and $\xi' = 1-\xi$ — evenly distributed random values within the interval [0, 1].

A similar inverse transform is applied to the cosine of the scattering angle: from the expression $\gamma = \cos\theta$ we obtain

$$\chi = 2\pi\int_{-1}^{\gamma} p(\gamma')d\gamma', \tag{8}$$

where $p(\gamma)$ — normalized phase function of scattering. The azimuthal angle ϕ is evenly distributed over the segment $[0, 2\pi]$. Thus, the three-dimensional integral with respect to the relative coordinate $\mathbf{r}'_j = \mathbf{r}_j - \mathbf{r}_{j-1}$ is transformed into the following form:

$$\int d\mathbf{r}'_j \Lambda(r'_j)p(t_j)f(r'_j,t_j) = \frac{1}{2\pi\mu}\int_0^1 d\xi_j\int_0^1 d\chi_j\int_0^{2\pi} d\phi_j \times f\left(-\mu^{-1}\ln\xi_j, t(\chi_j)\right), \tag{9}$$

where $f(r'_j, t_j)$ — is the arbitrary function, $t_j = t(\chi_j)$ — function inverse to the dependence $\chi_j = \chi(t_j)$ of (8), and ϕ_j — azimuthal angle. After such a transformation, the integral is calculated as the average of a sample of three uniformly distributed random variables: ξ, χ and ϕ, where the first two lie in the interval [0, 1], and ϕ — in $[0, 2\pi]$.

As a result, the intensity of n-th order $J^{(n)}(1, s_f)$ in the approximation of averaging over N_{ph} incident photons is found using the formula:

$$J^{(n)}(1,s_f) \simeq \sum_{i=1}^{N_{\text{ph}}} \frac{W_n^{(i)}}{N_{\text{ph}}} p\left(\mathbf{k}_f - \mathbf{k}^{(i)}_{n,n-1}\right) e^{-\mu s_f z_n^{(i)}}, \tag{10}$$

where $W_n^{(i)}$ — are the stochastic weights, and the sequence of points $\mathbf{r}_1, \ldots, \mathbf{r}_n$ defines the stochastic trajectory. The value $z_j^{(i)}$ indicates the distance from the jth scattering point to the boundary. The function $e^{-\mu s_f z_n^{(i)}}$ takes into account the attenuation of radiation during propagation from the last scattering point $z_n^{(i)}$ to the outer boundary of the medium.

An inhomogeneous medium is considered, the properties of which depend on the position along the Cartesian coordinate z perpendicular to the plane boundaries. Since the model does not take into account refraction at the layers interface, it is assumed that the direction of motion of the photon remains constant as it passes through the medium. In this case the decay exponential function moving from point $\mathbf{r}_0$ to point $\mathbf{r}$ is generalized as follows:

$$\exp\left(-\mu|\mathbf{r}-\mathbf{r}_0|\right) \longrightarrow \exp\left(-\frac{1}{\cos\theta}\int_{z_0}^{z}\mu(z')dz'\right), \tag{11}$$

where θ — the angle between the photon's direction of motion and z axis that shall be set in advance. Note that the final distribution depends on the initial position of the photon $\mathbf{r}_0$.

The probability density for the coordinate z, which determines the new position of the photon, is given by:

$$f(z,z_0) = C_0^{-1}\exp\left(-\frac{1}{\cos\theta}\int_{z_0}^{z}\mu(z')dz'\right), \tag{12}$$

where C_0 — is a normalization constant.

4. Modeling of multiple scattering

Let's calculate the skull curvature line. We will take a hemisphere of a given radius as the model of the head. Then, the skull layer (A) will be located between the two hemispheres of radii $R_{\max}$ and R_A. Thus, the layers are not located between planes, but between hemispheres. In point (0, 0, 0) the parietal bone is located. The equation of the surface of the head model in Cartesian coordinates has the following form:

$$x^2 + y^2 + (z - R_{\max})^2 = R_{\max}^2. \tag{13}$$

If we use spherical coordinates with the onset in point$(0, 0, R_{\max})$, then, the radius will change within $r_{\text{sph}} \in [0; R_{\max}]$, polar angle — within $\theta_{\text{sph}} \in [\pi/2; \pi]$, and azimuthal angle —within $\phi_{\text{sph}} \in [0; 2\pi]$. The curvature is taken into account through constraints on Cartesian coordinates: $x^2 + y^2 + (z - R_{\max})^2 \le R_{\max}^2$ and $z \in [0; R_{\max}]$. In this case, the attenuation coefficient μ depends on the radial distance r_{sph}:

$$r = -\mu^{-1}(r_{\text{sph}})\ln(1-\xi) = -\mu^{-1}(r_{\text{sph}})\ln\xi', \tag{14}$$

where ξ and $\xi' = 1-\xi$ are random variables evenly distributed over a segment $[0; 1]$.

In a 2-layer model:

layer A corresponds to the domain$R_{\max} \ge r_{\text{sph}} > R_A$,

layer B corresponds to domain $R_A \ge r_{\text{sph}} > 0$.

The algorithm shall take into account the successive stages that the photon passes, starting from the point r_0, going along the axis Z for a random distance (14). For a 2-layer model:

$$\mu(r) = \begin{cases} \mu_A, & R_{\max} \ge r > R_A, \\ \mu_B, & R_A \ge r > 0. \end{cases} \tag{15}$$

Then, random distance passed before scattering:

$$r = \begin{cases} -\mu_A^{-1}\ln(1-\xi), & \xi_A \ge \xi > 0, \\ -\mu_B^{-1}\left(\ln(1-\xi) + (\mu_B - \mu_A)(R_{\max} - R_A)\right), & 1 \ge \xi > \xi_A, \end{cases} \tag{16}$$

where $\xi_A = 1 - \exp\left(-\mu_A(R_{\max} - R_A)\right)$.

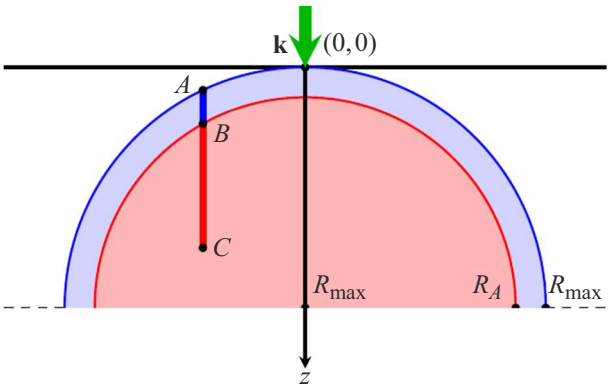

Figure 1. Schematic representation of calculating $l_j^{(i)}$.

The anisotropy of the medium is taken into account through the phase function $p(\cos\theta)$, where θ — single scattering angle. Henyey–Greenstein function is used [1]:

$$p_{\mathrm{HG}}(\cos\theta) = \frac{1}{4\pi}\frac{1-g^2}{(1+g^2-2g\cos\theta)^{3/2}}, \qquad (17)$$

where $g = \langle\cos\theta\rangle$ — anisotropy parameter. In both cases $g_A, g_B = g = 0.9$.

Integral function of distribution:

$$p_{\mathrm{HG}}(\cos\theta) = \int_{-1}^{\cos\theta} p_{\mathrm{HG}}(s)ds = \frac{1-g^2}{2g}\left(\frac{1}{\sqrt{1+g^2-2g\cos\theta}} - \frac{1}{1+g}\right), \qquad (18)$$

Inverse transform:

$$\cos\theta = \frac{1}{2g}\left(1+g^2-\frac{(1-g^2)^2}{(1-g+2g\chi)^2}\right), \qquad (19)$$

where χ — evenly distributed random value over $[0;1]$.

For the contribution of n-fold scattering into $J^{(n)}(1, s_f)$ intensity according to Monte Carlo method:

$$J^{(n)}(1, s_f) \simeq \sum_{i=1}^{N_{\mathrm{ph}}} \frac{W_n^{(i)}}{N_{\mathrm{ph}}} p\left(\mathbf{k}^f - \mathbf{k}_{n,n-1}^{(i)}\right) e^{-\mu s_f l_n^{(i)}}. \qquad (20)$$

Here $l_j^{(i)}$ — distance from j-th scattering event to the boundary. Since the medium is heterogeneous over r, this function is calculated based on the position of the scattering point $\mathbf{r}_{\mathrm{sph},n}^{(i)}$.

Fig. 1 illustrates how $l_j^{(i)}$ is defined if j-th event occurs in B layer. Based on coordinates $C(x_c, y_c, z_c)$ and radii $R_A, R_{\max}$:

$$AB = \sqrt{R_{\max}^2 - x_c^2 - y_c^2} - \sqrt{R_A^2 - x_c^2 - y_c^2}, \qquad (21)$$

$$BC = \sqrt{R_A^2 - x_c^2 - y_c^2} - R_{\max}. \qquad (22)$$

Table 1. Absorption coefficients μ_a (mm^{-1}) and reduced backscattering coefficients μ_s' (mm^{-1}) for various biological tissues at the given wavelength [31]

Biological tissue	Wavelength, λ							
	750 nm		850 nm		950 nm		1050 nm	
	μ_a	μ_s'	μ_a	μ_s'	μ_a	μ_s'	μ_a	μ_s'
Brain	0.036	0.859	0.106	0.762	0.114	0.622	0.118	0.525
Skull	0.006	1.974	0.013	1.876	0.019	1.757	0.019	1.665
Blood	0.530	0.725	0.720	0.649	0.930	0.650	0.560	0.645
Skin	0.046	1.535	0.038	1.485	0.030	1.625	0.022	1.695

If j-th event occurs in A layer, then:

$$l^{(i)}j = \sqrt{R_{\max}^2 - x_c^2 - y_c^2} - R_{\max}. \qquad (23)$$

Since we do not take into account the refraction at the boundary, it is assumed that the direction of the photon does not change when passing through the boundary. The exponential decay from the scattering point $\mathbf{r}$ to the boundary is described as:

$$e^{-\mu(r)\cdot l_n^{(i)}}. \qquad (24)$$

In this case, depending on the position of the scattering point:

$$e^{-\mu(r)\cdot l_n^{(i)}} = \begin{cases} e^{-\mu_A\left(\sqrt{R_{\max}^2 - x_c^2 - y_c^2} - R_{\max}\right)}, & r > R_A, \\ e^{-(\mu_A AB + \mu_B BC)}, & r \le R_A, \end{cases} \qquad (25)$$

where AB and BC are defined in the formulae (21) and (22).

5. Modelling subject to the layers curvature

This section presents the results of computational modeling of the intensity of near-infrared laser radiation backscattering in a two-layer biological medium. The optical parameters of the tissues used in the calculations are given in Table 1.

The modeling was performed using Monte Carlo method with the inverse transform of the cumulative distribution function of the photon mean free path [22]. Laser radiation was assumed to enter the medium along Z axis. In the process of multiple scattering, backscattering is formed, the contribution of which to the resulting intensity was recorded at each scattering point.

Since the model has cylindrical symmetry, the backscattering intensity was estimated on the surface of the hemisphere at a distance of ρ from Z axis. The calculations used

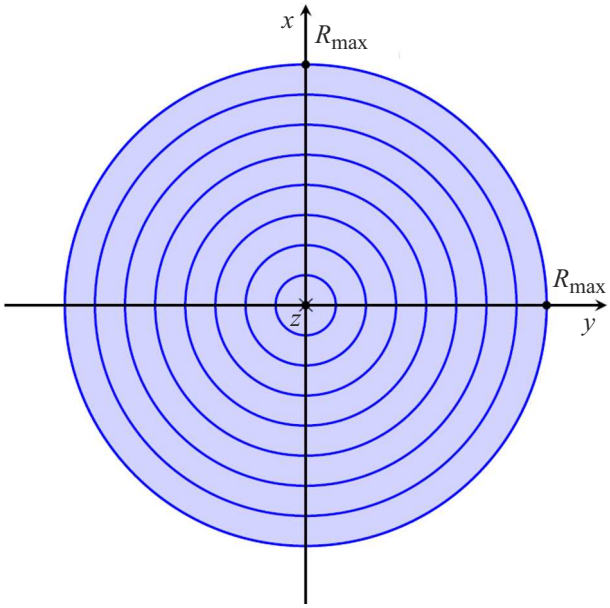

Figure 2. Schematic representation of the rings arrangement for easy counting (plan view).

a limit on the maximum number of scattering $n = 3 \cdot 10^5$ with a total number of photons $N_{ph} = 10^6$.

In biomedical optics, the reduced scattering coefficient $\mu_s' = (1 - g)\mu_s$ is often used, where g is the average cosine of the scattering angle. The values from Table 1 were used for modeling.

The purpose of the modeling is to determine the dependence of the logarithm of the intensity $\log_{10} J(\rho)$ on the radial distance ρ. The upper limit for ρ is chosen to be 40 mm, since at large distances the intensity decreases by more than 10 orders of magnitude compared to the central region ($\rho = 0$).

When registering backscattering, it was taken into account from which of the ring detectors the photon was „emitted". Fig. 2 shows the arrangement of the ring detection zones. This scheme allows aggregating the statistics by zones within certain radii. The hypothesis is that for sufficiently large radii, a model with the curvature of the layers should produce results close to the case of planar layers. To test this assumption, various environment configurations were modeled.

To determine the limits of applicability of the model used, a modeling of a single-layer system consisting of brain tissue was performed for various values of the scattering anisotropy parameter g. The criterion for the applicability of the model is the condition for the deviation of the integral backscattering intensity by no more than 10% relative to the base value: $|J/J_0 - 1| < 10\%$, where J — integral intensity at a given value of parameter g, and J_0 — value at $g = g_0 = 0.9$. The modeling results are shown in Fig. A10. They demonstrate the stability of the model in the range of values of the anisotropy parameter $g \in [0.85; 0.92]$.

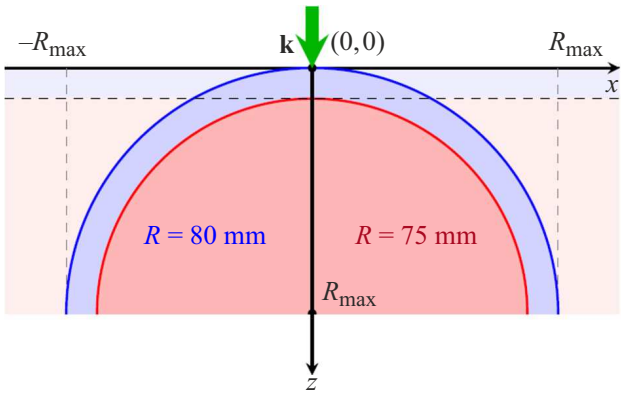

Figure 3. Schematic comparison of models with planar and spherical layers.

5.1. Modeling for a 2-layer biological tissue

From Figs. A1, A2 we may ascertain that the proposed hypothesis is true. Some differences are observed only at large ρ, but they can have an occasional nature. Next, let's find out at which radii the planar layers and hemispheres do not differ. Let's model three cases:

1. Planar layers with a thickness of $T = 150$ mm.
2. Spherical layers with a radius of $R_{max} = 150$ mm.
3. Spherical layers with a radius of $R_{max} = 80$ mm.

During modeling, it was found out that not a single photon from 10^6 was scattered below 150 mm. In this regard, we consider the planar layers with a thickness of $T = 150$ mm. Let's consider the scattering at various thicknesses of the A(skull) layer.

As can be seen from Fig. A1, A2, there are practically no differences, i.e. we can approximately consider spherical layers as planar.

5.2. Comparison of scattering modeling results in planar and spherical layer systems

One of the key tasks of this work is to study the effect of the curvature of the head hemispherical model on the intensity of backscattering. To do this, it is necessary to determine from which radius of the head the spherical model can no longer be approximately considered planar.

For analysis, we consider a single-layer model of bone tissue (A layer) at various radii R_{max}. The radius will gradually go down from 80 mm to 10 mm.

The analysis of the above graphs allows us to conclude that the effect of curvature on the backscattering intensity becomes noticeable at radii $R_{max} \leq 40$ mm. For large radii, the geometry of the layer can be approximated as planar.

Figure 3 provides a schematic illustration of the differences between models with planar and spherical layers.

Table 2. Absorption coefficients μ_a (mm^{-1}) and reduced scattering coefficients μ_s' (mm^{-1}) for CSF at various wavelengths

Biological tissue	Wavelength, λ							
	750 nm		850 nm		950 nm		1050 nm	
	μ_a	μ_s'	μ_a	μ_s'	μ_a	μ_s'	μ_a	μ_s'
CSF	0.002	0.001	0.004	0.001	0.039	0.001	0.016	0.001

According to the data [32], the human head contains about 100–150 ml of blood. In case of traumatic blood ingestion into CSF, three degrees of severity are distinguished depending on the volume of blood:

- Low — $V_{\text{blood}} \leq 50$ ml,
- Medium — $50 < V_{\text{blood}} \leq 100$ ml,
- High — $V_{\text{blood}} > 100$ ml.

Let's consider how the presence of blood in CSF layer affects the intensity of backscattering. For this, the corresponding values of the optical absorption coefficients μ_a and the reduced scattering coefficient μ_s' for blood are used [11].

6. Influence of the radius of curvature of the model on the calculation results in a four-layer model

Let's consider an enlarged model consisting of four layers: skin (A), skull (B), CSF (C) and brain (D). Below are the results of modeling the backscattering intensity of laser radiation versus the distance ρ between the registration point and Z axis.

Additionally, we will analyze the effect of the presence of blood in CSF, which may occur, for example, with traumatic brain injury.

Let us assume that:

- layer A: domain $R_{\max} \geq r > R_A$;
- layer B: domain $R_A \geq r > R_B$;
- layer C: domain $R_B \geq r > R_C$;
- layer D: domain $R_C \geq r > 0$.

Then, the function of the attenuation coefficient $\mu(r)$ is set as follows:

$$\mu(r) = \begin{cases} \mu_A, & R_{\max} \geq r > R_A, \\ \mu_B, & R_A \geq r > R_B, \\ \mu_C, & R_B \geq r > R_C, \\ \mu_D, & R_C \geq r > 0. \end{cases} \quad (26)$$

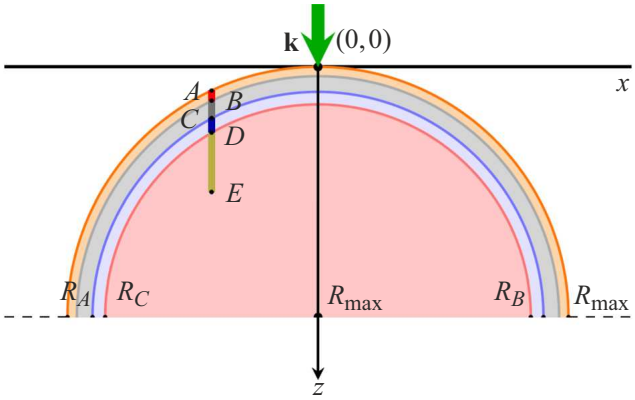

Figure 4. Schematic representation of calculating $l_j^{(i)}$ in case of four layers.

The path of a photon and its interaction with the medium depend on the optical characteristics of each layer through which it passes between scattering events.

Parameters of anisotropy g for various tissues shall be assumed equal:

- $g_A = 0.9$ — skin [2];
- $g_B = 0.9$ — bone [22];
- $g_C = 0.98$ — CSF [33];
- $g_D = 0.9$ — brain [34].

In Fig. 4 the general distance from the initial point to the point of j-th scattering AE includes sequential regions: $AE = AB + BC + CD + DE$. Using the coordinates of the scattering point $E(x_E, y_E, z_E)$ and the set values of the layer boundaries, the lengths of these segments can be determined similarly to the formulae (21), (22).

As in the case of the two-layer model, the calculations take into account the exponential decay of radiation in accordance with Bouguer–Lambert–Beer law.

The modeling was carried out similarly to a two-layer system. The number of permitted events of scattering was $n = 3 \cdot 10^5$, and the total number of photons was — $N_{\text{ph}} = 10^6$.

Special attention is paid to the scenario where blood penetrates into the CSF layer. In this case, the attenuation coefficient μ for the layer C is recalculated based on the percentage of blood:

$$\mu_C = (1 - \alpha)\mu_{\text{CSF}} + \alpha\mu_{\text{blood}},$$

where α — portion of blood in the volume of CSF.

Because, as shown in sec. 3, the modeling results for $R_{\max} = 80$ mm and $R_{\max} = 150$ mm are almost identical, the value $R_{\max} = 80$ mm is used further, which corresponds to the average radius of an adult human head. The thicknesses of the layers A, B and C were calculated to be 3, 7, and 2 mm, respectively.

In Fig. A8 and A9 it is shown that the presence of blood in CSF significantly reduces the backscattering intensity at distances of more than 20 mm from the radiation entry point. This is due to the fact that at short distances the main contribution to backscattering is made by the upper layers of the head, whereas at long distances the contribution from the inner and outer layers becomes comparable.

To assess the threshold sensitivity of the model, various concentrations of blood in CSF were analyzed. The results showed that when the blood content is more than 10%, there is a noticeable change in the intensity of backscattering, especially at distances of more than 30 mm from the entry point. This makes promising the use of this method for noninvasive detection of intracranial hemorrhages by the rate of decrease in the intensity of backscattered laser radiation with increasing distance between the detector and entry point of the laser beam. However, today the authors don't know if any of such approaches have been implemented so far in the noninvasive diagnostics.

7. Conclusion

The computational modeling of the intensity of infrared laser radiation backscattering for biological tissues represented as a two-layer and four-layer randomly inhomogeneous medium was carried out. Two geometric approximations are considered: a model of planar layers of finite thickness and a model of hemispherical layers imitating the shape of a human head. The model does not take into account variations in the thickness of the skin and bone layers, which depend on the anatomical area of the head and the age of the person. The difference in skin pigmentation, which can significantly affect the modeling results, is also neglected.

The accuracy of the calculated parameters was controlled by the stability of numerical values with the higher sampling size. With a sample size of 10^6 , the backscattering intensity remains stable with an accuracy of at least four significant digits. However, to provide the accuracy comparable with the other results the data shown in Fig. A8, A9 may require higher sampling size by two-three orders of magnitude. Nevertheless, even with reduced accuracy, the obtained dependences make it possible to reliably assess the nature of changes in the studied quantities.

The major focus is made on a 2-layer model of „skull–brain" and 4-layer model of „skin–skull–CSF–brain". The influence of the curvature of a head model on backscattering was investigated.

The modeling results show that the curvature has a significant effect on the backscattering intensity at detection radii less than 40 mm. At large distances, the deviations become negligible, which makes it possible to use a simplified model with plane layers without significant loss of accuracy.

Additionally, the effect of the presence of blood in CSF in the context of modeling a intracranial injury was considered. It was demonstrated that when the volumetric concentration of blood in CSF exceeds 10%, significant changes in the characteristics of backscattering were observed. This can be used for non-invasive diagnostics of intracranial injuries and hemorrhages.

Conflict of interest

The authors declare no conflict of interest.

Appendix

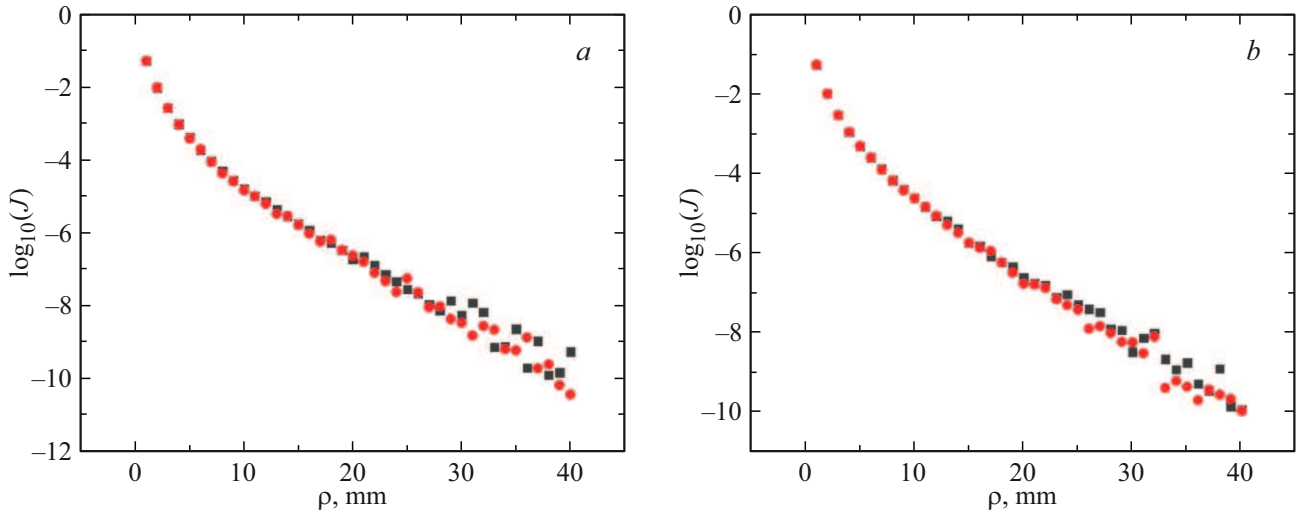

Fig. A1. Intensity of backscattering in a two-layer model of the skull (A) and brain (B) versus source–receiver distance. Layers thickness for plane layers $T_{\text{full}} = 150$ mm, and $R_{\max} = 150$ mm for spherical layers. Thicknesses of layer $T_A = 3$ mm (a) and $T_A = 5$ mm (b). ■ — spherical layers, • — plane layers.

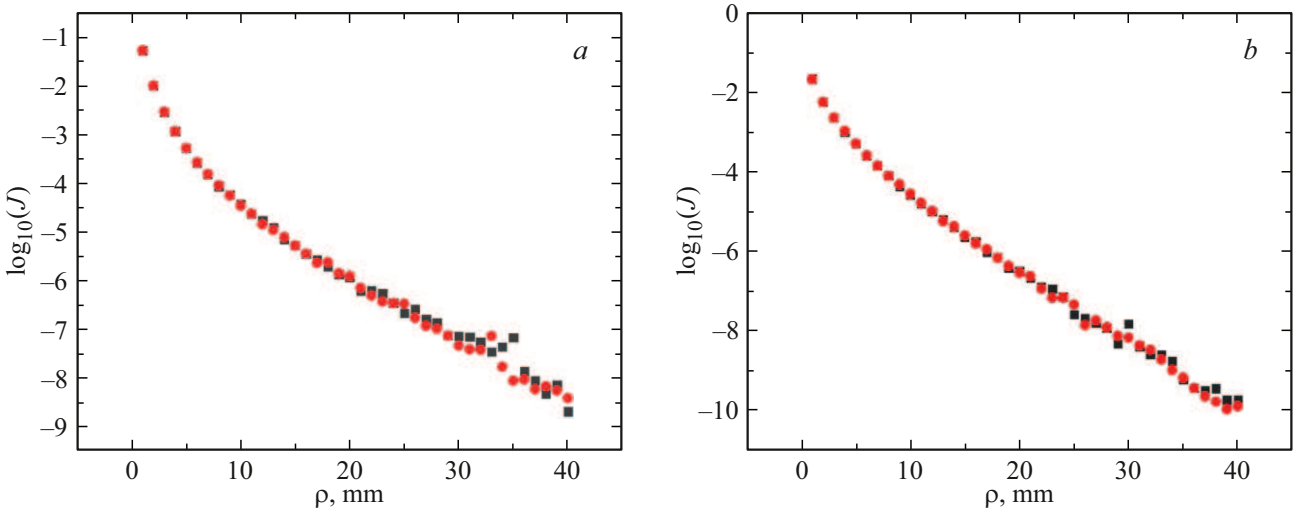

Fig. A2. Intensity of backscattering in a one-layer model of bone tissue (a) and brain (b) versus source−receiver distance. Layers thickness for plane layers $T_{\text{full}} = 150$ mm, radius of spherical layers $R_{\max} = 150$ mm: ■ — spherical layers, ● — plane layers.

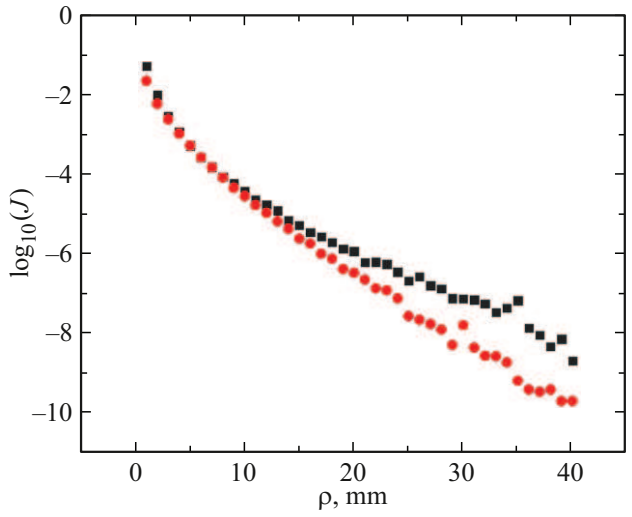

Fig. A3. Intensity of backscattering in a one-layer model of spherical layers ($R_{\max} = 150$ mm) versus source−receiver distance: ■ — bone tissue, ● — brain.

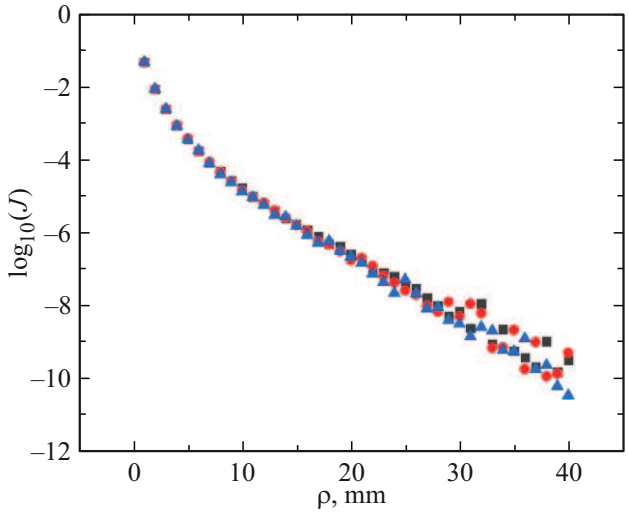

Fig. A4. Intensity of backscattering in a two-layer model of the skull (A) and brain (B) versus source-receiver distance for the layer thickness $T(A) = 3$ mm in three cases: ■ — $R_{\max} = 80$ mm, ● — $R_{\max} = 150$ mm, ▲ — $T = 150$ mm.

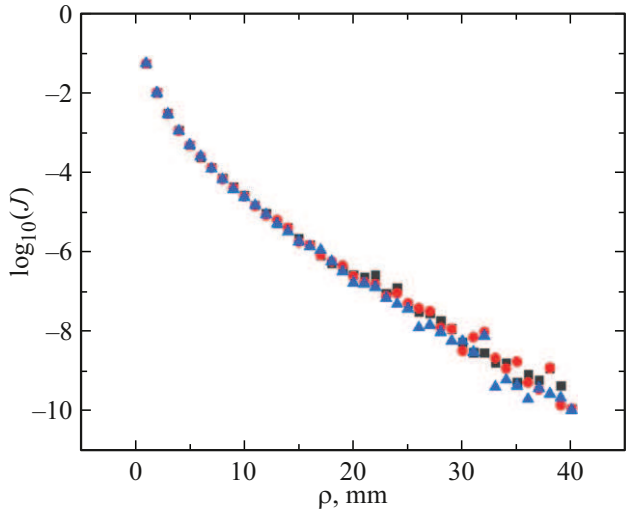

Fig. A5. Intensity of backscattering in a two-layer model of the skull (A) and brain (B) versus source−receiver distance for the layer thickness $T(A) = 5$ mm in three cases: ■ — $R_{max} = 80$ mm, ● — $R_{max} = 150$ mm, ▲ — $T = 150$ mm.

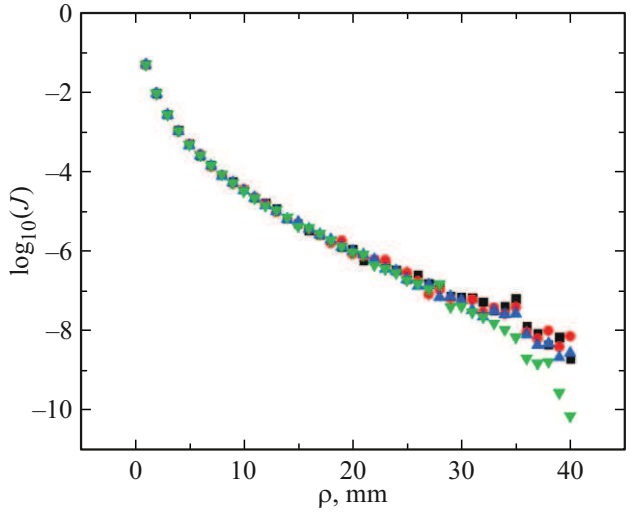

Fig. A6. Intensity of backscattering in a bone tissue hemisphere versus source−receiver distance at various radii: ■ — $R_{max} = 150$ mm, ● — $R_{max} = 80$ mm, ▲ — $R_{max} = 60$ mm, ▼ — $R_{max} = 40$ mm.

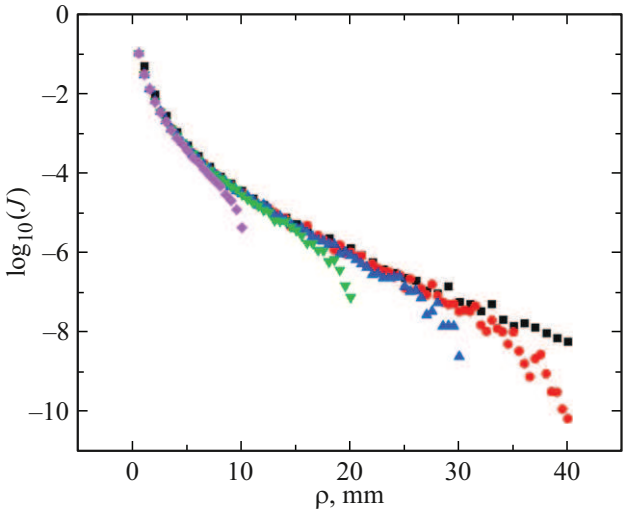

Fig. A7. Intensity of backscattering in a bone tissue hemisphere versus source−receiver distance at various radii: ■ — $R_{max} = 150$ mm, ● — $R_{max} = 40$ mm, ▲ — $R_{max} = 30$ mm, ▼ — $R_{max} = 20$ mm, ♦ — $R_{max} = 10$ mm.

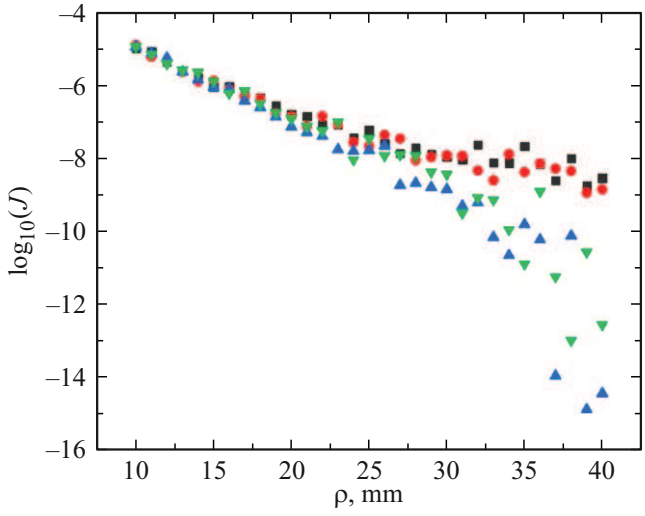

Fig. A8. Intensity of backscattering in a four-layer model: skin (A), skull (B), CSF (C), brain (D) versus source-receiver distance at various concentrations of blood in the CSF: ■ — plane layers (0%), ● — hemispherical layers (0%), ▲ — plane layers (100%), ▼ — hemispherical layers (100%).

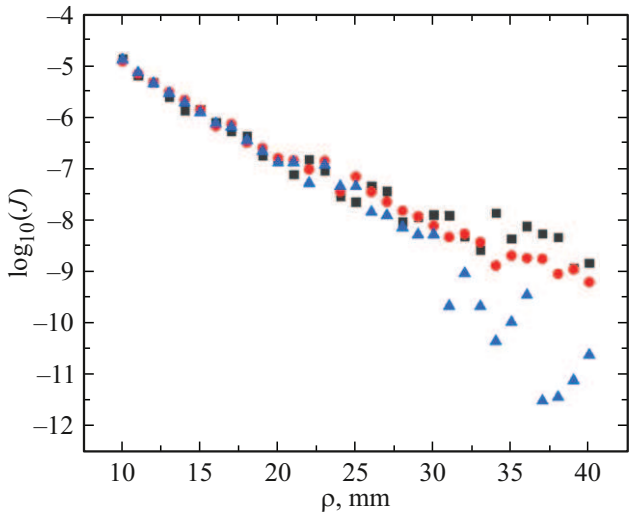

Fig. A9. Intensity of backscattering in a four-layer model: skin (A), skull (B), CSF (C), brain (D) versus source-receiver distance at various concentrations of blood in the CSF: ■ — 0%, ● — 10%, ▲ — 50%.

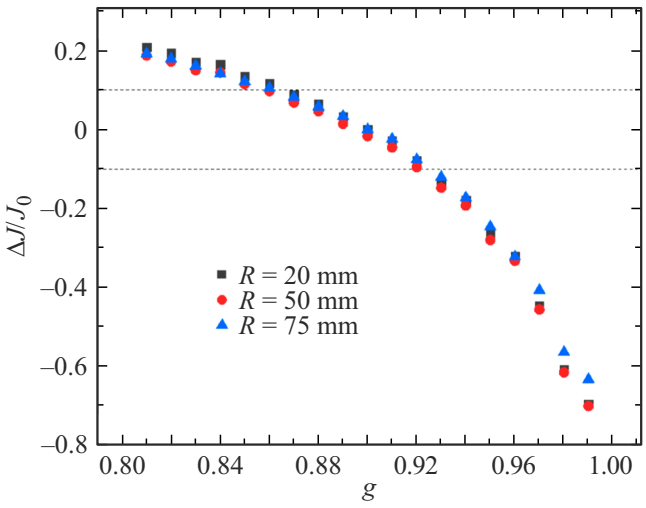

Fig. A10. Deviation of the integral backscattering intensity versus the key value $J_0(g) = J(g_0)$, where $g_0 = 0.9$, in a single-layer system consisting of brain tissue, at different values of the anisotropy parameter g. Three curves for different surface curvature values are shown.

References

[1] V.V. Tuchin. *Optika biologicheskikh tkanei. Metody rasseyaniya sveta v meditsinskoy diagnostike* (IPR Media, M., 2021).

[2] S.L. Jacques. Phys. Med. Biol., **58**, R37 (2013). DOI: 10.1088/0031-9155/58/11/R37

[3] F. Scholkmann, S. Kleiser, A.J. Metz, R. Zimmermann, J. Mata Pavia, U. Wolf, M. Wolf. Neuroimag., **85**, 6 (2014). DOI: 10.1016/j.neuroimage.2013.05.004

[4] H. Liu, D.A. Boas, Y. Zhang, A.G. Yodh, B. Chance. Phys. Med. Biol., **40**, 1983 (1995). DOI: 10.1088/0031-9155/40/11/015

[5] O. Pucci, V. Toronov, K. St Lawrence. Appl. Opt., **49**, 6324 (2010). DOI: 10.1364/AO.49.006324

[6] V.L. Kuzmin, Yu.A. Zhavoronkov, S.V. Ul'yanov, A.Yu. Valkov. J. Exp. Theor. Phys., **134**, 661 (2022) (in Russian). DOI: 10.31857/S0044451022060013

[7] D.T. Delpy, M. Cope. Philos. Trans. R. Soc. B Biol. Sci., **352** (1354), 649 (1997).

[8] V. Ntziachristos, B. Chance. Med. Phys., **28**, 1115 (2001). DOI: 10.1118/1.1373674

[9] A. Torricelli, D. Contini, A. Pifferi, M. Caffini, R. Re, L. Zucchelli, L. Spinelli. Neuroimage **85**, 28 (2013).

[10] A. Kienle, M.S. Patterson, N. Dögnitz et al. Appl. Opt., **37** (4), 779 (1998).

[11] H. Wabnitz, J. Rodriguez, I. Yaroslavsky, A. Yaroslavsky, V.V. Tuchin. Handbook of Optical Biomedical Diagnostic Light-Tissue Interaction, 2-nd ed. (SPIE Press, Bellingham, Washington, 2016). Vol. 1, 784 p.

[12] M.S. Patterson, B. Chance, B.C. Wilson. Appl. Opt., **28** (12), 2331 (1989).

[13] J. Zhao, H.S. Ding, X.L. Hou, C.L. Zhou, B. Chance. J. Biomed. Opt., **10**, 024028 (2005). DOI: 10.1117/1.1891345

[14] T. Durduran, R. Choe, J.P. Culver, L. Zubkov, M.J. Holboke, J. Giammarco, B. Chance, A.G. Yodh. Phys. Med. Biol., **47**, 2847 (2002). DOI: 10.1088/0031-9155/47/16/302

[15] M.A. Franceschini, S. Thaker, G. Themelis, K.K. Krishnamoorthy, H. Bortfeld, S.G. Diamond, D.A. Boas, K. Arvin, P.E. Grant. Pediatr. Res., **61**, 546 (2007). DOI: 10.1203/pdr.0b013e318045be99

[16] S. Fantini, M. A. Franceschini, J.S. Maier, S.A. Walker. Opt. Eng. **34** (1), 32 (1995).

[17] S. Mahmoodkalayeh, M.A. Ansari, V.V. Tuchin. Biomed. Opt. Express, **10**, 2795 (2019).

[18] M.S. Cano-Velazquez, N. Davoodzadeh, D. Halaney et al. Biomed. Opt. Express, **10**, 3369 (2019).

[19] Yu.A. Zhavoronkov, S.V. Ul'yanov, A.Yu. Valkov, V.L. Kuzmin. Pisma v ZhETF, **117** (5), 389–396 (2023) (in Russian).

[20] M.C.W. Van Rossum, Th.M. Nieuwenhuizen. Rev. Mod. Phys., **71**, 313 (1999).

[21] V.L. Kuzmin, I.V. Meglinskii. Quantum Electronics, **36** (11), 990–1002 (2006).

[22] L. Wang, S.L. Jacques, L.Q. Zheng. Comput. Meth. Prog. Bio., **47**, 131 (1995).

[23] V.L. Kuzmin, I.V. Meglinsky. Opt. and spectr., **97** (1), 108–115 (2004) (in Russian).

[24] V.L. Kuzmin, I. Meglinski. Opt. Commun. **273** (2), 307–310 (2007).

[25] I. Meglinski, V.L. Kuzmin et al. Proc. Roy. Soc. A, **461**, 43–53 (2005).

[26] V.L. Kuzmin, I.V. Meglinsky. Pisma v ZhETF, **79** (3), 139–142 (2004) (in Russian).

[27] V.L. Kuzmin, A.Yu. Val'kov. Pisma v ZhETF **105**, 261 (2017) (in Russian).

[28] V.L. Kuz'min, A.Yu. Val'kov, L.A. Zubkov. ZhETF **155**, 460 (2019) (in Russian). DOI: 10.1134/S0044451019030088

[29] V.L. Kuzmin, V.P. Romanov, E.V. Aksenova. Phys. Rev. E, **65**, 016601 (2001). DOI: 10.1103/PhysRevE.65.016601

[30] T.M. Nieuwenhuizen, J.M. Luck. Phys. Rev. E, **48** (1), 569 (1993). DOI: 10.1103/PhysRevE.48.569

[31] R. Francis, B. Khan, G. Alexandrakis, J. Florence, D. MacFarlane. Biomed Opt Express, **6** (9), 3256–3267 (2015).

[32] B.L.C. Wright, J.T.F. Lai, A.J. Sinclair. J. Neurol., **259**, 1530–1545 (2012).
[33] A. Roggan. J. Biomedical Optics, **4**(1), 36–46 (1999). DOI: 10.1117/1.429919
[34] A.N. Yaroslavsky et al. Phys. Med. Biol., **47**, 2059 (2002). DOI: 10.1088/0031-9155/47/12/305

Translated by J.Savelyeva